LANGMUIR

pubs.acs.org/Langmuir Article

In Situ Nanostructural Analysis of Concentrated Wormlike Micellar Fluids Comprising Sodium Laureth Sulfate and Cocamidopropyl Betaine Using Small-Angle Neutron Scattering

Ashley P. Williams, Joshua P. King, Anna V. Sokolova, Liliana de Campo, and Rico F. Tabor*

Cite This: https://dx.doi.org/10.1021/acs.langmuir.0c02530 Read Online

ACCESS | Metrics & More | Article Recommendations | Supporting Information

ABSTRACT: Concentrated wormlike micellar fluids form the basis for a vast array of formulated products, from liquid soaps and shampoos to drag reduction and drilling fluids. Typically, these systems are analyzed using bulk rheological measurements to determine their flow properties and cryo-microscopy to detect their nanostructure. Small-angle neutron scattering provides an opportunity to directly and nonperturbatively analyze nanostructure *in situ* but is complicated for concentrated systems by correlations from interparticle volume exclusion. Here, we use small-angle and ultra-small-angle neutron scattering to probe directly for the first time the nanostructure of concentrated wormlike micellar fluids composed of the widely used surfactant pair sodium laureth sulfate and cocamidopropyl betaine in aqueous electrolytes. Obtained data are analyzed using different approaches to determine scattering contributions from the wormlike particles themselves and interactions between them. It is found that approximating worms as locally rigid cylinders offers some insight into their aggregation dimensions at short length scales, and both volume exclusion and screened Coulombic interaction potentials describe interactions reasonably well. Using the semi-empirical polymer reference interaction site model (PRISM) gives excellent agreement with observed scattering, and physical insight obtained using this approach is discussed in detail. A drawback of this method is the significant complexity in coding the model in order to fit data, so to facilitate this for future researchers, we provide with this paper a fully operational, open-source code to utilize this model.

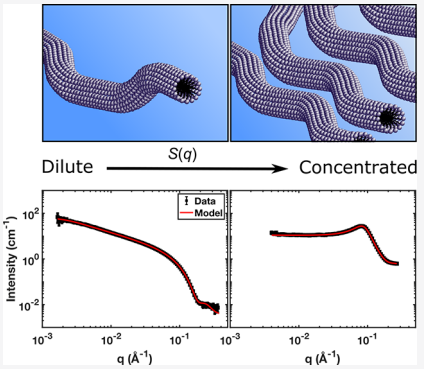

INTRODUCTION

Background. Surfactants are known for their ability to aggregate into different morphologies as a result of their amphiphilic structure. These morphologies can also be manipulated by the addition of cosurfactants, counterions, and electrolytes to form particularly interesting and exotic architectures such as wormlike micelles (WLMs),[1−3] disk-like micelles,[4,5] or even hamburger-like micelles.[6] Of particular interest are WLMs, which underpin the formulation of many complex fluids, from personal care products such as shampoos,[7] through to fracturing fluids,[8,9] drag reduction agents,[10] and viscosity modifiers.[11] More recently, stimulus responsiveness has been targeted in order to modulate WLM rheology in the presence of light, CO_2, or changes in pH.[12−14] Depending on the specific surfactants used and their concentrations, WLMs typically have very large aspect ratios, with diameters of only a few nanometers and lengths of several micrometers, allowing for polymer-like complex fluid behaviors above the micelle overlap concentration C^*,[3] most notable of which is viscoelasticity.

Two techniques that are typically applied to study WLM fluids are (1) rheology, to identify flow characteristics and macroscale properties such as viscosity and storage and loss moduli (G' and G''), and (2) neutron scattering, to determine the mesoscale architecture including cross-sectional radius r_{cs}, contour length L, Kuhn length b (twice the persistence length, *i.e.*, the length over which the micelle is effectively rigid), and radial polydispersity.[15−17] Together, these techniques describe the relevant characteristics of micellar systems, yet to date, there is no systematic method for predicting rheological values from neutron scattering data or vice versa. Understanding the structure of WLMs at surfactant concentrations above the overlap concentration is therefore a crucial step in linking the mesoscale structure to macroscale rheology.

A particularly widely used wormlike micellar fluid comprises a mixture of anionic surfactant sodium laureth sulfate (SLES) and zwitterionic surfactant cocamidopropyl betaine (CAPB, Figure 1a) in an aqueous electrolyte (generally sodium chloride). This mixture has found use in a vast array of personal and home care products from liquid soaps and shower gels to household and automotive cleaning fluids. In these

Received: August 27, 2020
Revised: November 3, 2020

https://dx.doi.org/10.1021/acs.langmuir.0c02530
Langmuir XXXX, XXX, XXX−XXX

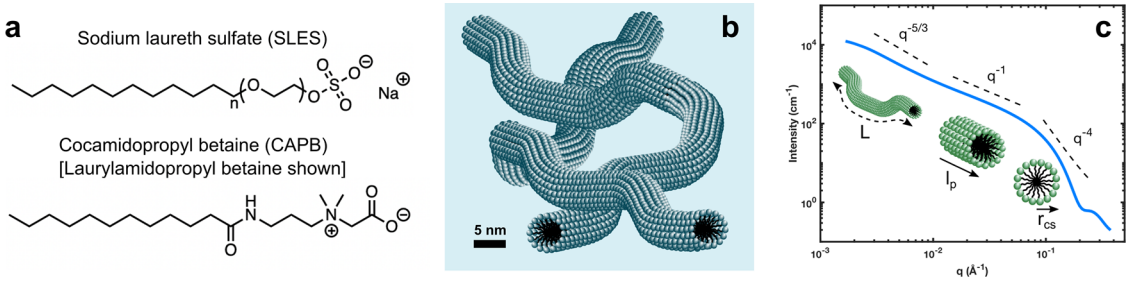

Figure 1. (a) Chemical structures of sodium laureth sulfate (SLES) and laurylamidopropyl betaine, the main and prototypical component of cocamidopropyl betaine (CAPB). (b) Schematic showing wormlike micelles formed by a concentrated mixture of SLES and CAPB, above the critical overlap concentration, C^*. (c) Schematic of a small-angle scattering pattern showing a dilute wormlike micellar system, indicating main correlation regions.

applications, the surfactant loading is typically on the order of 10−30 wt %. The rheology of this system across a wide range of concentrations from semidilute to highly concentrated, including response to various additives, is well understood. It is therefore surprising that scattering measurements at industrially relevant concentrations (>5 wt %) have not been performed on this system, or indeed any analogous wormlike micellar system, as these would allow valuable correlations between nanostructure and bulk properties to be made. We posit that this arises primarily from a difficulty in quantitatively analyzing obtained scattering data.

Previous scattering studies of SLES/CAPB systems indicate persistence lengths of 600 Å, for dilute (0.2 wt %) WLMs in 3−5 wt % electrolyte and with relatively large uncertainties in modeled contour lengths (±900 − 10,000 Å).[18] Rheological studies identified a sharp peak in the zero-shear viscosity for 10 wt % SLES/CAPB with a mass ratio of 34:66 without the electrolyte, indicative of a wormlike transition.[19] The addition of electrolyte promotes the formation of WLMs at lower surfactant concentrations,[18] and above a critical electrolyte concentration, semidilute solutions form a branched network that exhibits a significantly reduced viscosity.[19] Above the dilute surfactant regime, the low-q scattering gradient flattens with increasing surfactant concentration due to the additional inter-worm volume exclusion.[20]

In the present work, we explore the nanostructure of concentrated wormlike micellar fluids (up to 30 wt % surfactant) comprising SLES and CAPB in a 0.3765 M sodium chloride solution, *in situ* using small- and ultrasmall-angle neutron scattering, as well as polarizing light microscopy. We highlight physical insight into micellar dimensions that can be obtained by modeling scattering data in different ways and provide an outlook for this and other wormlike systems at high volume fractions.

EXPERIMENTAL METHODS

Materials. This work employs a series of samples comprising CAPB, SLES, and sodium chloride (NaCl) as model wormlike systems. CAPB was freeze-dried (LabConCo Freezone 2.5) from an obtained stock solution (Aussie Soap Supplies "Coco Betaine", 30−50% in H_2O, 5.8−7.3% NaCl present) and was resdissolved and centrifuged twice from dry methanol to ensure NaCl was removed. Residual NaCl content was tested by the addition of 3.0 mM $AgNO_3$ to a dissolved sample of CAPB. No turbidity/precipitate was observed, indicating that only trace NaCl remained. SLES was also freeze-dried from an obtained stock (New Directions Australia, 68−72% in H_2O). SLES and CAPB were dissolved in D_2O to form 30 wt % stocks. These stocks were then systematically stirred together before the addition of 0.3765 M NaCl.

Small- and Ultra-small-Angle Neutron Scattering (SANS/USANS). Small-angle neutron scattering (SANS) data were obtained using the Bilby beamline in time-of-flight mode at the Australian Centre for Neutron Scattering (ACNS), ANSTO, Lucas Heights, NSW, Australia.[21,22] Measurements were conducted at 25 °C in a 1 mm total path length couette cell for the 15, 20, and 25 wt % samples. The detector setup was able to yield a q range of 0.0040 − 0.2802 $Å^{-1}$. The detector setup for the 1−10 wt % samples, in demountable quartz cells, was able to yield a q range of 0.0017 − 0.5032 $Å^{-1}$. Incident neutrons had wavelengths of 2−18 Å. An empty beam measurement and the sample thickness (1 mm for 15−25 wt %, 2 mm for 1−10 wt %) were used to scale the absolute intensities measured.

Ultra-small-angle neutron scattering (USANS) data were obtained on the Kookaburra beamline, ACNS, with an incident neutron wavelength λ = 4.74 Å.[23] Kookaburra is a Bonse−Hart instrument, utilizing two quintuple-reflection channel-cut perfect silicon crystals as a monochomator and analyzer. Demountable quartz cells (1 mm path length) were utilized for USANS measurements. Samples were prepared in D_2O for optimal contrast. SANS data were smeared to match the USANS before the data were stitched together and desmeared.[24] Comparison of desmeared SANS data to the SANS data before being smeared ensured that the desmearing process had produced the correct results. Model fitting for cylinder, flexible cylinder, and fractal models were performed using the software "SasView" (http://sasview.org) for all neutron scattering data. PRISM was implemented in the program "MATLAB" (http://mathworks.com) from the flexible cylinder model and amended, as described in detail in the Supporting Information.[1,2,25] A scattering length density of 1.0 × 10^{-6} $Å^{-2}$ for the micelle was used here to simplify calculations for this mixed surfactant system. The precise SLD of CAPB and SLES is around 0.381 × 10^{-6} $Å^{-2}$ for each of the main species present (laurylamidopropyl betaine and sodium lauryl monoethoxy sulfate, respectively), but solvent (D_2O) penetration into the micelle core, headgroup hydration, and high salt concentration all contribute to reducing this contrast slightly; hence, a value of 1.0 × 10^{-6} $Å^{-2}$ was chosen in order to remain consistent and simplify calculations throughout.

Polarizing Light Microscopy (PLM). Polarizing light microscopy (PLM) images were obtained using a CCD camera (Flea3, Point Grey, Richmond, BC, Canada) coupled to a polarizing light microscope (Kozo XJP-300). Samples were placed on glass microscope slides and covered with a coverslip. Slides were then placed on a temperature-controlled sample stage (Peltier temperature stage, Linkam Scientific PE120, linked to a recirculating water bath with an accuracy of ±0.1 °C) and thermally annealed to remove any alignment induced by sample preparation before images were taken.

RESULTS AND DISCUSSION

At a fundamental level, small-angle scattering describes correlations between particles (in the case of neutron scattering, nuclei), where contrast is induced by differences between the scattering length of nuclei. Here, this is achieved

https://dx.doi.org/10.1021/acs.langmuir.0c02530
Langmuir XXXX, XXX, XXX−XXX

by deuteration of the solvent (D_2O) in order to provide contrast for the hydrocarbon surfactant tails and to some extent for the surfactant head groups also. In aggregating systems, the specific spatial arrangement of atoms in molecules and the arrangement of molecules into ordered structures such as micelles result in a constructive and destructive interference that, when summed across all orientations, results in the detected scattering pattern. The scattered intensity as a function of the scattering vector, q, therefore describes the extent of correlation at different length scales, and by comparing this to model predictions for how different structures and geometries should scatter, parameters describing aggregate geometry and interactions can be obtained. The situation is complicated by the convolution of scattering arising from correlations within structures that describe the shape and size of aggregate structures (that is, the scattering form factor, $P(q)$) and scattering due to correlations arising from local ordering between structures, generally at higher concentrations (the structure factor, $S(q)$).

In the case of wormlike micelles (Figure 1b), the separation between form and structure factors is complicated by the unique geometry of these aggregates. At small length scales (medium to high q), scattering correlations are dominated by locally rigid cylindrical sections of the micelles, and this region of the scattering pattern ($q > 0.02$ Å^{-1} for the system investigated here) is well described by a cylindrical form factor in dilute conditions. This form factor results in a scaling of intensity at intermediate q values of the form $I \propto q^{-1}$ (Figure 1c). At larger length scales (lower q), scattering becomes dominated by an intraparticle structure factor contribution in the form of a random self-avoiding walk, identical to that obtained from the polymer theory and resulting in a limiting gradient where $I \propto q^{-5/3}$. In cases where the overall contour length of the worm is sufficiently small as to be resolved by SANS, the scattering pattern may flatten off ($I \propto q^0$) at lowest q, although this is rarely the case, generally reflecting total micelle lengths >1 μm. Small-angle scattering data for wormlike systems at low concentrations (where only intra-worm volume exclusion needs to be accounted for) can be modeled using a semi-analytical flexible cylinder model that accounts for these geometric factors by asymptotically matching the form factor for a cylinder at high q to the self-avoiding walk structure factor contribution at low q.[2] At higher concentrations where interworm volume exclusion (*i.e.*, scattering correlations between neighboring worms) are important, this model must be augmented using an additional approximate structure factor contribution.[1,25]

SANS data obtained from the wormlike micellar system of CAPB/SLES (66:34 mass ratio) at a range of concentrations in 0.3765 M aqueous NaCl were fit using the flexible cylinder model (including intra-worm, single-particle volume exclusion, but not inter-worm, many particle volume exclusion), as indicated in Figure 2; fitting parameters are provided in Table S1 of the Supporting Information. We note here that CAPB/SLES (66:34) micelles in 0.3765 M NaCl are not wormlike below 1 wt % surfactant loading and hence, the fluid concentrations shown in this work begin at 1 wt %. It is evident that the fit is reasonable at low concentrations (1 wt %) but rapidly deviates as the surfactant volume fraction is increased, most notably at lower-q. Note that micelle lengths provided are a lower bound as SANS cannot resolve micelle contour length for these systems. Previous studies have indicated that micellar length increases with concentration

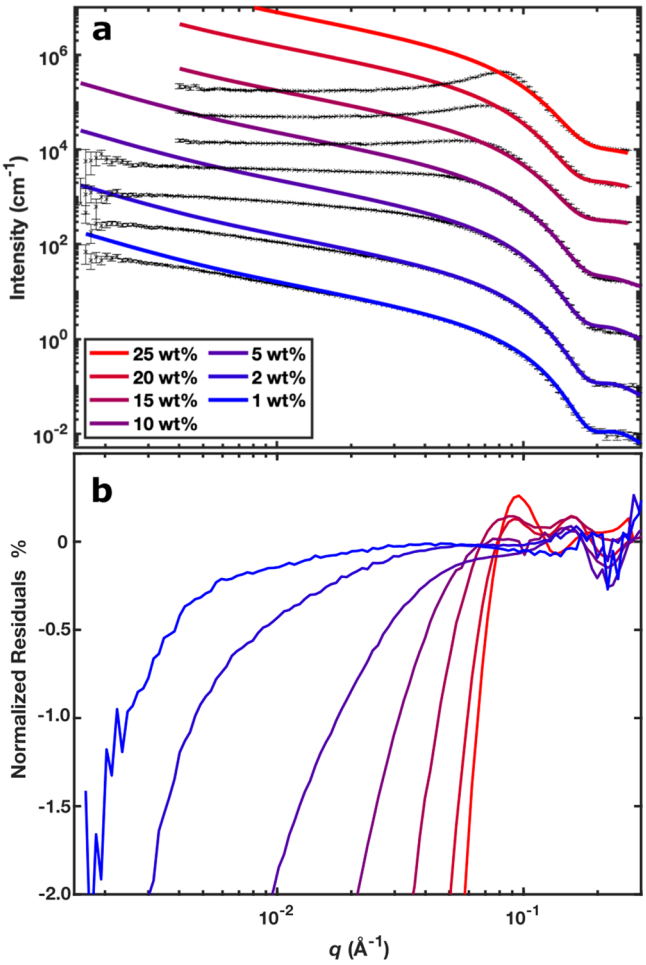

Figure 2. (a) Experimental SANS (symbols) and flexible cylinder model fits (solid line) for SLES/CAPB (34:66) in 0.3765 M NaCl. Fits and data have been offset by a factor of 5^0, 5^1, ..., 5^6 for clarity. (b) Normalized residuals indicating the deviation between data and fit for the flexible cylinder model.

for these systems.[3] This is as anticipated based on the discussion above, indicating the rapid dominance of inter-worm scattering contributions in the form of a large structure factor peak, as predicted by Cannavacciuolo *et al.*[1] The high-q region ($q > 0.1$ Å^{-1}) is reasonably described by the cross-sectional cylindrical form factor P_{CS}, but deviation is noted even in this region at high surfactant concentrations as the model is unable to describe the structure factor peak. The deviations between the model and obtained scattering data are particularly evident in the normalized residuals shown in Figure 2b, indicating the growing and systematic deviation between the model and data.

Due to the lack of an explicit inter-micellar structure factor, it is clear that the flexible cylinder model cannot describe scattering from concentrated surfactant samples. This is noted repeatedly in the literature,[26−30] where this additional structure factor is not accounted for in model fits. However, the cross-sectional cylindrical regime at high q fits the data comparatively well, as expected. Hence, in the following sections, we seek to determine whether simple (and easier to calculate) correlation models can be used to extract physical insight from these systems over a limited q-range.

The flexible cylinder model contains the cylindrical form factor P_{CS} given in eq S10, (Supporting Information), so here,

https://dx.doi.org/10.1021/acs.langmuir.0c02530
Langmuir XXXX, XXX, XXX−XXX

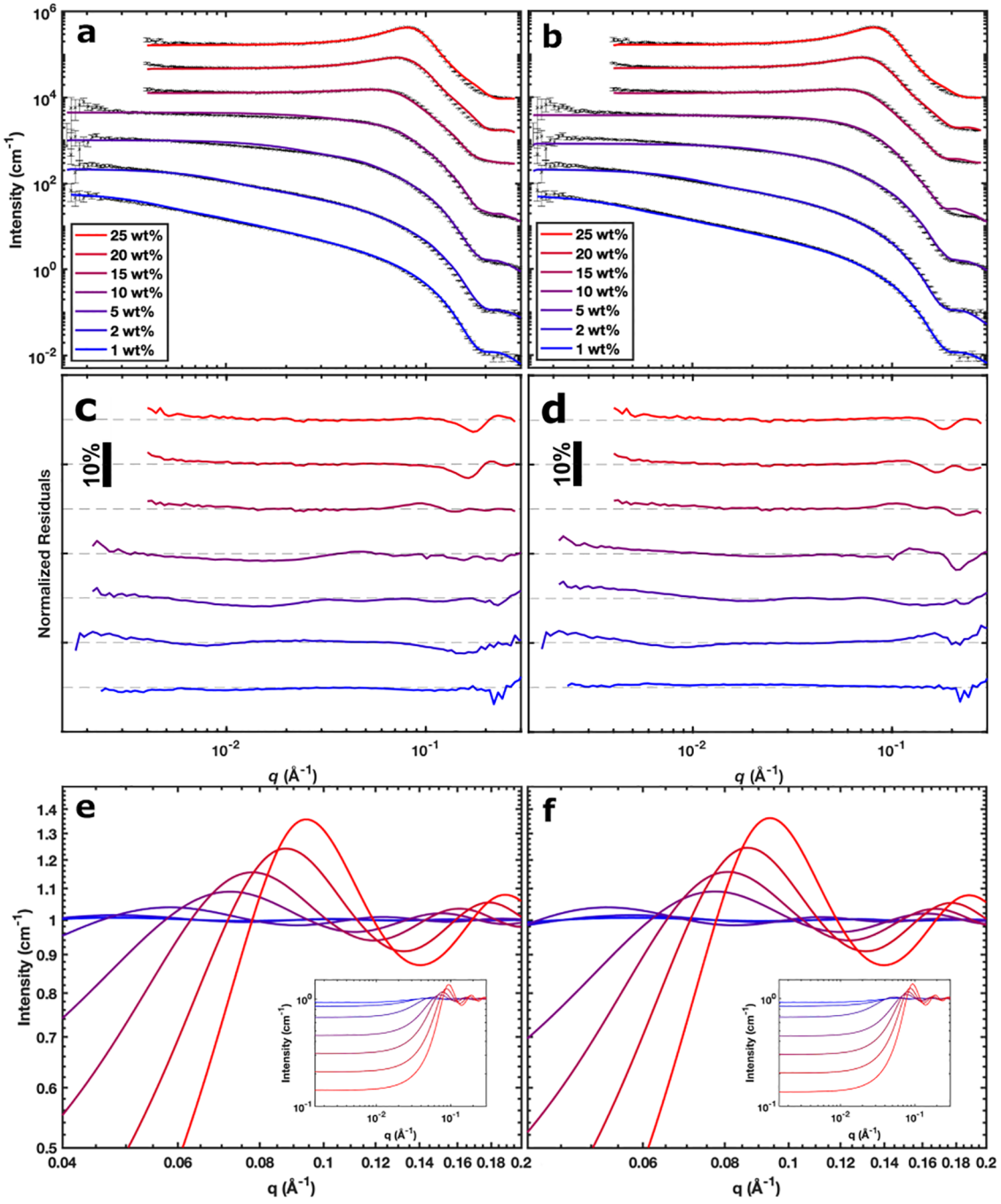

Figure 3. (a) Experimental SANS (symbols) and rigid cylinder model with hard sphere structure factor fits (solid line) for SLES/CAPB (34:66) in 0.3765 M NaCl. Fits and data have been offset by a factor of 5^0, 5^1, ..., 5^6 for clarity. (b) Experimental SANS (symbols) and rigid cylinder model with HPMSA structure factor fit (solid line) for SLES/CAPB (34:66) in 0.3765 M NaCl. Fits and data have been offset by a factor of 5^0, 5^1, ..., 5^6 for clarity. (c, d) Normalized residuals indicating the deviation between data and fit for the rigid cylinder model with (c) hard sphere structure factor and (d) HPMSA structure factor. (e) Hard sphere structure factor contribution to fits from (a), where the inset shows the full q range. (f) HPMSA structure factor contribution to fits from (b), where the inset shows the full q range

we expect to be able to accurately represent the cylindrical cross section of our wormlike micellar systems at higher q. This raises the question of how relevant scattering contributions arising from micelle connectivity (*i.e.*, intraparticle volume exclusion) are at higher volume fractions. It is reasonable to hypothesize that connectivity becomes less important to the overall scattering signal as volume fraction increases, and therefore, intra-worm scattering contributions increase. The question remains of which structure factor to use for this specific system of SLES/CAPB micelles. The addition of hard sphere volume exclusion can represent the structure factor of a system if there is no electrostatic interactions between particles (micelles). A Hayter−Penfold mean spherical approximation can represent a structure factor of a system if there are electrostatic interactions between micelles; if the net charge of the particles approaches zero, then this structure factor reduces to the hard sphere structure factor case. Although a pure volume exclusion structure factor contribution can be

https://dx.doi.org/10.1021/acs.langmuir.0c02530
Langmuir XXXX, XXX, XXX−XXX

renormalized to account for cylindrical geometries, the Hayter–Penfold MSA structure factor cannot, and so we would anticipate its accuracy to decrease as aspect ratio of the cylindrical subsections increases.

Approximating Wormlike Micelle Scattering as Cylinders with Hard Sphere and Hayter–Penfold MSA Structure Factors. By approximating WLMs as an ensemble of rigid cylinders (where cylinders represent locally rigid sections of the WLMs), we anticipate that agreement at low q may be weak. In this region, correlations at larger length scales due to micellar connectivity become important, and these will not be well described by uncorrelated individual cylinders. However, this may be less important at higher micelle volume fractions where inter-micellar structure factor contributions dominate. At mid- to high q, we anticipate that a rigid cylinder with appropriate structure factor contribution should describe WLMs well. Due to added salt, the CAPB/SLES systems studied here had a Debye length (κ^{-1}) of approximately 4.94 Å, indicating that charge contributions to structure factor interactions are minimal and highly screened. Nonetheless, we applied both hard sphere (HS) and Hayter–Penfold mean spherical approximation (HPMSA) charged structure factor models to the scattering data for comparison and to highlight the role of the charge component. The fitting parameters are given in Table S2 of the Supporting Information.

It is evident from Figure 3 that both the cylinder–HS and cylinder–HPMSA models produced a higher quality fit and better agreement with the experimental data when compared to the flexible cylinder model, particularly as the structure factor contribution became more prominent. These fits did show some deviation at low q, as expected, evidenced particularly in the residuals plots (Figure 3c,d). Also as anticipated, these models do not resolve the contour length of the WLMs and instead indicate the length of locally rigid micelle sections that decreased from 1200 Å at 1 wt % surfactant to 57–58 Å at 25 wt %. This interesting observation may indicate a limitation of this modeling approach or an increase in tortuosity or lowering of correlation length within the cylindrical micelle sections as the micelle volume fraction increases. Further, as the hard sphere structure factor begins to dominate, the model becomes less sensitive to cylinder length.

Both models did however yield appropriate values of the effective radius r_{eff} and were able to fit with approximate volume fractions, ϕ. The distinction between radius r and effective radius r_{eff} in neutron scattering is important here. As utilized in the present modeling, r refers to the radius of the micelle at the contrast step, *i.e.*, the radius of the micellar hydrocarbon core, as we anticipate that the highly hydrated head groups have a contrast similar to the bulk D_2O solvent. Effective radius, r_{eff}, corresponds to the radius used in structure factor calculations, *i.e.*, the radius at which the micelles interact with one another. This therefore accounts for the head group region and potentially also for some additional size due to bound ions and/or hydration. For cylindrical subunits, r_{eff} can be calculated in a number of ways, for example from the average curvature of the shape or the equivalent volume sphere. As hypothesized earlier, fits using the cylinder–HPMSA model were very similar when compared to the cylinder–HS model due to the very short range electrostatic interactions that contribute minimally to interactions. Fit parameters for the HPMSA structure factor contribution such as charge therefore are likely to have large margins of error, and we do not discuss or interpret them in detail here for this reason. Since these models do not account for the self-avoiding walk nature of WLMs, their structural parameters describing larger length scales cannot be analyzed or interpreted. The structure factor contributions do however suggest that scattering from the WLMs is dominated by spatial confinement/volume exclusion at higher concentrations.

Modeling concentrated WLMs as uncorrelated cylinders clearly faces some limitations, and so the alternative approach of using the flexible cylinder model modified with an approximation for the direct correlation function $\beta c(q)$ is explored.

Polymer Reference Interaction Site Model (PRISM) Fitting and Analysis. The PRISM model to describe concentrated wormlike chain systems was explored by Cannavacciuolo *et al.*,[1] resulting in an approximate form of the direct correlation function, $\beta c(q)$. Explicit description of the equations used to describe the scattering function are provided in the Supporting Information of the present work and more fully in ref 1. In applying this model, it should be noted that the direct correlation function approximation was obtained by closed-form Monte Carlo simulations of wormlike chains at different concentrations, explicitly accounting for excluded volume interactions and thereby obtaining an empirically excellent agreement with experimental scattering data. Nonetheless, this derivation means that obtained parameters are empirical in nature, and their explicit relationship with physical quantities is not yet clear.

Here, we employed the PRISM model to describe obtained SLES/CAPB scattering data for concentrated wormlike systems (Figure 4). Both visually and numerically (by means of a reduced χ^2_R indicating goodness of fit), agreement was better using the PRISM model than using rigid cylinder models for all samples. By setting B as a fit parameter, it was not possible to yield a unique fit due to a proportional relationship between B and the flexible cylinder contour length L.[25] The fits were therefore obtained by using a ratio of $\frac{B}{L}$ as a fitting parameter, and these ratiometric values are supplied in Table S3 in the Supporting Information. As concentration increased, Kuhn length (a measure of persistence length, see Appendix) remained insensitive to the fitting and hence was fixed at 900 Å. Micelle radii and effective radii obtained from the three models are summarized in Figure 5; other parameters of the model are given in the Supporting Information.

Using the PRISM model, we observed an effective radius that was initially not defined at low concentrations (1 and 2 wt %, and hence was set equal to the micelle radius here) but at 5 wt %, the effective radius peaked at 65 ± 1.6 Å. As surfactant concentration increased, the effective radius was reduced to 46.5 ± 0.2 Å. Along with this reduction in effective radius, as surfactant concentration increased, the radius of the micelles also decreased slightly (from 22.0 to 19.5 Å). All three models suggested a decrease in the effective radius and radius for the WLMs and we suspect that this is a compression effect of the micelles due to confinement of WLMs in the system. The reduction in effective radius is also suspected to be partly attributed to the confinement of micelles overcoming the weak electrostatic repulsions between each other. This is a result of the slight increase in charge screening effects from the increased proportion of charge present in the system from the added surfactant.

The ratio of PRISM to HS structure factors (Figure 6b) indicates the difference in peak positions for the intermicellar

https://dx.doi.org/10.1021/acs.langmuir.0c02530
Langmuir XXXX, XXX, XXX–XXX

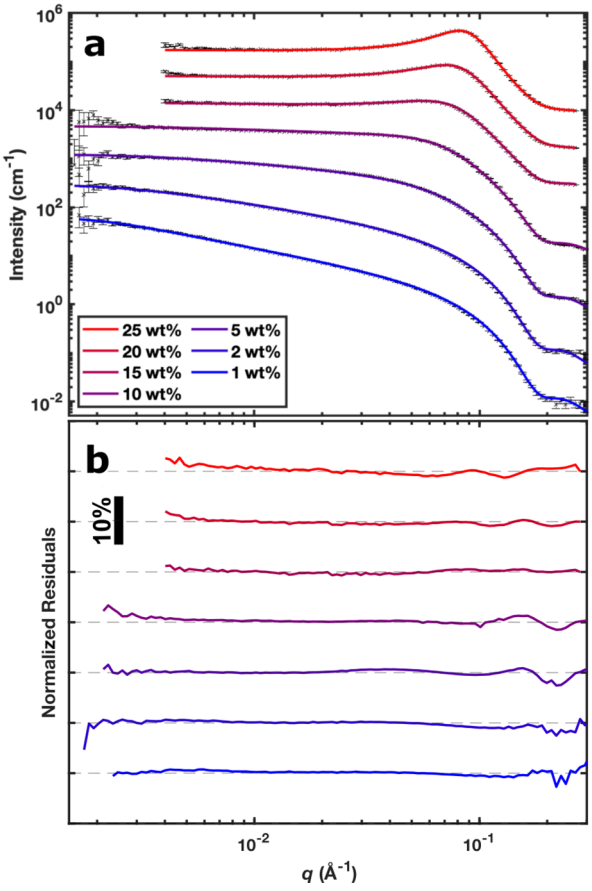

Figure 4. (a) Experimental SANS (symbols) and flexible cylinder−PRISM fits (solid line) for SLES/CAPB (34:66) in 0.3765 M NaCl. Data and fits are offset by 5^0,5^1, ...,5^6 for 1 to 25 wt % surfactant concentrations, respectively, for clarity. (b) Normalized residuals indicating the deviation between data and fit for the flexible cylinder−PRISM model.

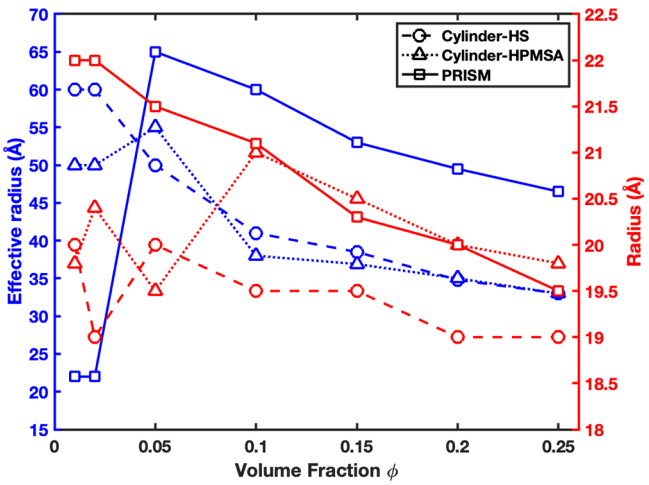

Figure 5. Change in micelle radii and effective radii for SLES/CAPB wormlike micelles at increasing volume fractions for the tested models (cylinder-HS and cylinder-HPMSA) and PRISM.

structure factor as seen by the peak shapes, between $10^{-2} < q < 10^{-1}$ Å^{-1}. Deviations at low q are dominated by the PRISM structure factor. The difference in intensity ratios for PRISM/HS and HPMSA/HS is noted, with larger oscillations in intensity seen for the PRISM structure factor, which was able

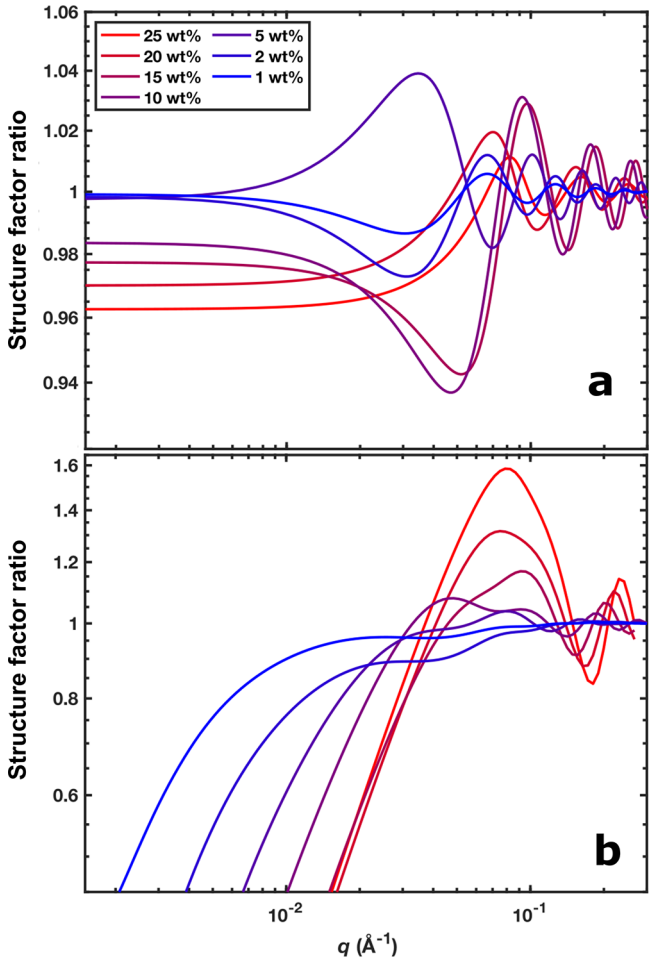

Figure 6. Ratios of (a) HPMSA and HS structure factors and (b) PRISM and HS structure factors to indicate their contribution to fitting concentrated wormlike neutron scattering data.

to more accurately fit concentrated WLM scattering data. The peak shape, while slightly influenced by the division of the HS structure factor, correlates to the increasing peak intensity (with surfactant concentration) seen in the SANS data. When compared to Figure 6b, the ratio of the HPMSA and HS structure factors (Figure 6a) indicates that these two contributions (HPMSA and HS) are almost identical, as anticipated for these highly screened systems: HPMSA essentially collapses to volume exclusion, with only small deviations.

To further explore the physical basis of the structure factor contribution from PRISM fitting, we compared this to an experimentally obtained pseudostructure factor S_{pseudo} given by

$$S_{pseudo}(q) \approx \frac{I_{conc}(q)}{I_{dil}(q)} \approx \frac{[S_{exv}(q) + S_{flex}(q)]P_{CS}(q, r)S_{obs}/A_{conc}}{[S_{exv}(q) + S_{flex}(q)]P_{CS}(q, r)/A_{dil}} \quad (1)$$

where A is the scale derived from PRISM fitting, composed of c and M, and S_{obs} is the observed structure factor contribution given by the scattering of a concentrated surfactant sample. Figure 7a presents pseudostructure factors derived experimentally, by the division of intensity values of high surfactant concentration scattering data by the intensity values of the lowest surfactant concentration where we observed wormlike

https://dx.doi.org/10.1021/acs.langmuir.0c02530
Langmuir XXXX, XXX, XXX−XXX

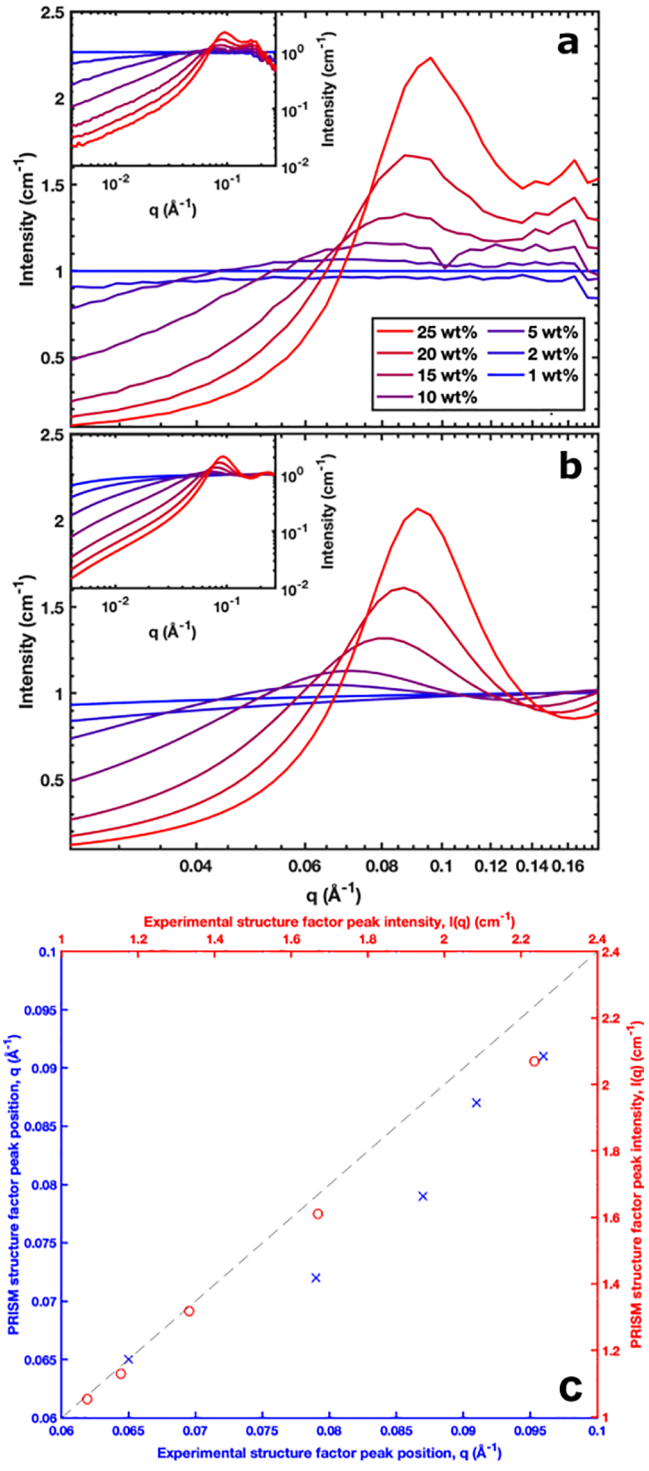

Figure 7. (a) Experimentally derived pseudostructure factor, S_{pseudo}. (b) Model derived structure factor, S_{PRISM}. (c) Comparison of peak positions and peak intensities between experimentally and PRISM derived structure factors (for 5−25 wt % samples), where the dotted line indicates agreement between the two.

behavior (1 wt %), given in eq 1. The other set of structure factors, as seen in Figure 7b, was derived from modeling with PRISM by extracting the structure factor in the form

$$S_{PRISM} = \frac{1}{1 + \beta c(q)[S_{exv}(q) + S_{flex}(q)]} \quad (2)$$

A strong correlation is evident between the respective structure factor functions in Figure 7, notably the peak intensities given in both the experimentally and PRISM-derived structure factors. Figure 7c highlights that while PRISM yielded appropriate intensities for each sample, it slightly underestimated the peak positions by approximately 0−0.01 Å^{-1} when compared to the experimentally derived structure factors. The approximation for the direct correlation function made by $\beta c(q)$, (eq S14, Supporting Information), is well supported by the similar peak positions and peak magnitudes in both structure factor function sets in Figure 7 and is appropriate for modeling the scattering where $q > 0.05$ Å^{-1}.

To determine values for contour length and the parameter B, the methods by Bonneté *et al.* (eq 2)[31] and Chen *et al.*[25] were employed by finding $S(0)$ from the experimentally derived structure factors. From the scattering observed by the SLES/CAPB samples, the $S(0)$ values could not be reliably chosen, with not all samples each converging to a singular intensity. It was found that the $S(0)$ values were severely overestimated and hence, the contour lengths were severely underestimated—assuming 700 Å in length for the most concentrated WLM solutions. It was not possible to employ this methodology for scattering observed in the ultra low-q regime explored via USANS (as mentioned in the next section) due to higher order structuring of the WLMs convoluting the scattering pattern.

From previous literature observations, it is expected that as surfactant concentration increases, wormlike micelle overall contour length increases.[3,32] However, this is not easily obtained from small-angle scattering measurements due to the limitation of the measurement length scale (typically <200 nm, whereas wormlike micelle total contour length is typically on the order of μm). Both rigid and flexible cylinder models suggest that the apparent length of the cylindrical units comprising the micelles decreases as the volume fraction increases, contrary to expectation.[11] This highlights the important and wide-ranging issue with scattering from WLM systems, where the ability to accurately measure contour length is generally inhibited by the limited q range of the measurement. Thus, we next explored whether correlations at larger length scales (smaller q), obtained using USANS measurements, could provide further insight.

Low-q Scattering of Concentrated WLMs from Ultra-small-Angle Neutron Scattering (USANS). It is of particular interest to interpret larger length scale structuring of wormlike micellar systems, which may yield an insight into how structure controls rheological properties such as storage and loss moduli or viscosity.[28] Here, we have utilized USANS to investigate the region $q \approx 10^{-5} - 10^{-3}$ Å^{-1}.

These scattering data could not be fit using any combination of (flexible) cylinder and structure factor model, indicating that beyond the dilute regime, correlations between neighboring wormlike micelles dominate scattering at greater length scales. This is logical based on the discussion above and indicates the failure of present analytical models in this region. Instead, data were fit using a mass fractal model, with a fractal dimension of 3.00, with the exception of the 25 wt % surfactant sample, corresponding broadly to a power law of the form $I(q) = q^{-D}$, where the power index indicates the fractal dimension, D (Table 1).[33]

We anticipate that this fractal model is a reasonable approximation of densely packed WLMs as we predict a

https://dx.doi.org/10.1021/acs.langmuir.0c02530
Langmuir XXXX, XXX, XXX−XXX

Table 1. Fitting Parameters from Fractal Fits of SLES/CAPB USANS Data

conc.	vol. frac. ϕ	domain size (Å)	dimension, D
2 wt %	0.02	$1.45 \times 10^4 \pm 1.26 \times 10^3$	3.0
5 wt %	0.05	$1.59 \times 10^4 \pm 3.29 \times 10^2$	3.0
10 wt %	0.10	$2.20 \times 10^4 \pm 2.12 \times 10^2$	3.0
15 wt %	0.15	$2.30 \times 10^4 \pm 5.00 \times 10^4$[a]	3.0
20 wt %	0.20	$2.37 \times 10^4 \pm 4.72 \times 10^2$	3.0
25 wt %	0.25	$2.63 \times 10^4 \pm 1.02 \times 10^2$	2.9

[a]Domain size varied significantly with slight adjustments in the fractal model. This is suspected to be due to the desmearing process for this sample.

hierachial structure of WLMs or regions of local order that appear self-similar over several decades of q. Most locally, volume exclusion results in alignment or bundling of WLMs with one another, as has been seen using cryo-TEM.[34,35] These "bundles" may form domains that look self-similar at larger length scales (in a similar fashion to liquid crystalline domains, although likely less ordered). Here, we obtained an indication of correlated domains on the order of 10^4 Å, which approaches the length scale that we can observe using visible light. Figure 8c highlights the ordering of a 30 wt % SLES/CAPB (34:66) sample using a polarizing light microscope. This birefringence texture indicates that there is local ordering of WLMs on the length scale of visible light, whereas the 25 wt % sample did not display any birefringence indicating that the ordered domains of WLMs below 30 wt % surfactant loading are smaller than can be observed with visible light or insufficiently ordered as to induce visible birefringence. This likely suggests that at 30 wt %, the WLMs are permanently aligned with respect to one another, at least locally, but below this concentration instead of equilibrium alignment, samples instead experience shear-induced alignment.[30]

CONCLUSIONS

In this work, we obtained small-angle neutron scattering data from wormlike micellar fluids ranging from dilute to concentrated and explored the physical insight that could be obtained by applying various geometric approximations to describe their scattering. The wormlike micelles (WLMs) studied comprised the widely researched and utilized combination of cocamidopropyl betaine and sodium laureth sulfate (CAPB/SLES) in aqueous sodium chloride solution.

It is clear that at surfactant concentrations above 1 wt %, scattering is rapidly dominated by a growing intermicellar structure factor contribution, and this can be described at high q by approximating the micelles as rigid cylinders interacting via either a volume exclusion or screened Coulombic interaction potential. Using the polymer reference interaction site model (PRISM) utilizing a flexible cylinder form factor closely reproduced experimental scattering data, with similar structure factor peak positions (within ± 0.1 Å^{-1}) and intensities. PRISM yielded physically reasonable effective radii (up to 60 Å) for these model WLMs; however, limitations arose when determining the values of the interaction parameter, B. It was not possible to utilize scattering at lower q (*i.e.*, in the USANS regime) due to the presence of additional contributions from longer-range correlations in concentrated systems, indicating that obtaining unique and accurate values of B and micellar contour length in concentrated systems may not be possible using current theoretical tools.

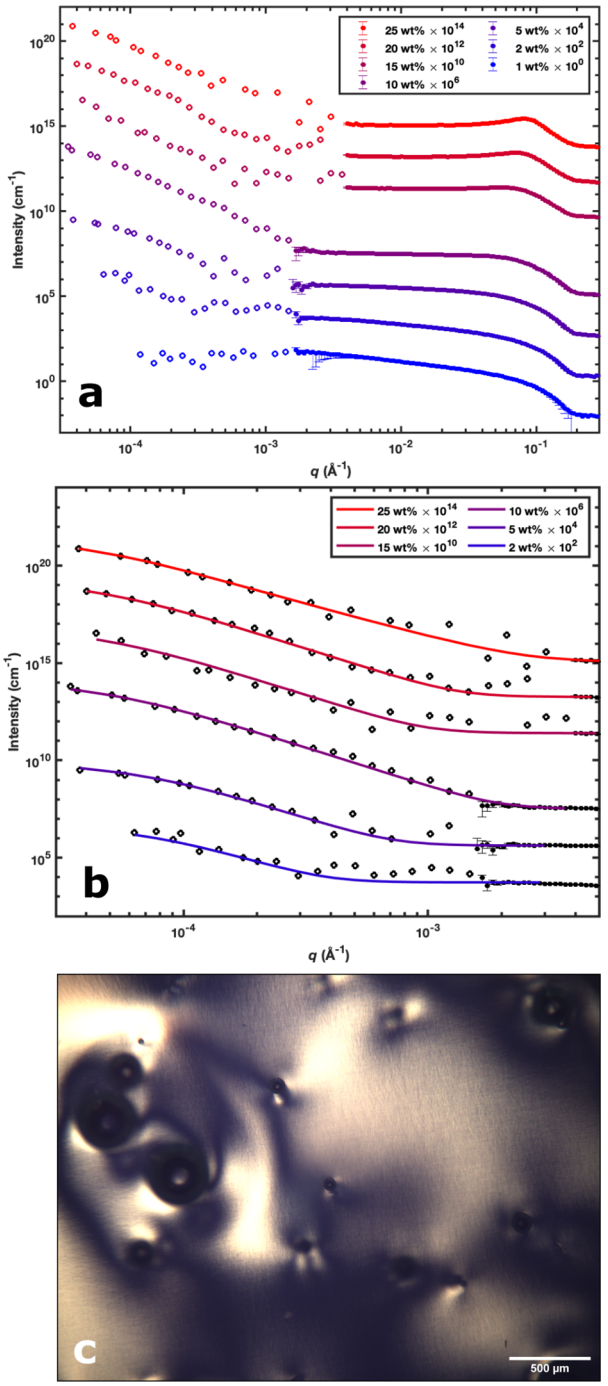

Figure 8. (a) Combined SANS and USANS data for SLES/CAPB (34:66) in 0.3765 M NaCl. Data have been vertically offset by multiplication as indicated for clarity. USANS data are denoted by hollow symbols, and SANS data are indicated by solid symbols. (b) Experimental USANS (hollow symbols) and fractal fits (solid line) for SLES/CAPB (34:66) in 0.3765 M NaCl. (c) Birefringence texture of 30 wt % SLES/CAPB (34:66) in 0.3765 M NaCl obtained using a polarizing light microscope in transmission mode.

All three models for SANS data indicated a slight reduction in micellar core radius (22 Å → 19.5 Å) of the SLES/CAPB WLMs as concentration increased, indicating closer or denser packing, potentially due to the modest increase in ionic strength or changes in surfactant chemical potential.

https://dx.doi.org/10.1021/acs.langmuir.0c02530
Langmuir XXXX, XXX, XXX−XXX

Comparisons using an approximate cylinder model with a volume exclusion structure factor closely resembled the fitting produced by PRISM, suggesting that charge was negligible in these highly screened systems. The WLMs also displayed further correlations at low q, indicating a fractal-like nature at $q = 10^{-5} - 10^{-3}$ Å^{-1}, with fractal dimension $D = 2.9 - 3.0$, suggesting that the WLMs form domains on the order of 10^4 Å in size. Once the concentration of surfactant reached 30 wt %, the sample became permanently birefringent, indicative of persistent, ordered domains on the length scale observable with visible light, suggesting equilibrium alignment of WLMs or a "locked-in" local structure.

■ ASSOCIATED CONTENT

Supporting Information

The Supporting Information is available free of charge at https://pubs.acs.org/doi/10.1021/acs.langmuir.0c02530.

PRISM code for modeling of wormlike micelle/polymer solutions (TXT)

Fitting parameters for SANS modeling of wormlike micellar systems; fitting models; and appendices (PDF)

■ AUTHOR INFORMATION

Corresponding Author

Rico F. Tabor − *School of Chemistry, Monash University, Clayton, VIC 3800, Australia;* orcid.org/0000-0003-2926-0095; Phone: +61 3 9905 4558; Email: rico.tabor@monash.edu; Fax: +61 3 9905 4597

Authors

Ashley P. Williams − *School of Chemistry, Monash University, Clayton, VIC 3800, Australia*

Joshua P. King − *School of Chemistry, Monash University, Clayton, VIC 3800, Australia*

Anna V. Sokolova − *Australian Centre for Neutron Scattering, ANSTO, Lucas Heights, New South Wales 2234, Australia*

Liliana de Campo − *Australian Centre for Neutron Scattering, ANSTO, Lucas Heights, New South Wales 2234, Australia;* orcid.org/0000-0003-4799-2935

Complete contact information is available at: https://pubs.acs.org/10.1021/acs.langmuir.0c02530

Notes

The authors declare no competing financial interest.

■ ACKNOWLEDGMENTS

We acknowledge the support of ANSTO in providing the neutron facilities used in this work. The work was supported by the AINSE Honours scholarship program, by an Australian Government Research Training Program (RTP) Scholarship, and by the Australian Research Council (Future Fellowship FT160100191).

■ REFERENCES

(1) Cannavacciuolo, L.; Pedersen, J. S.; Schurtenberger, P. Monte Carlo Simulation Study of Concentration Effects and Scattering Functions for Polyelectrolyte Wormlike Micelles. *Langmuir* **2002**, *18*, 2922−2932.

(2) Pedersen, J. S.; Schurtenberger, P. Scattering functions of semiflexible polymers with and without excluded volume effects. *Macromolecules* **1996**, *29*, 7602−7612.

(3) Dreiss, C. A. Wormlike micelles: Where do we stand? Recent developments, linear rheology and scattering techniques. *Soft Matter* **2007**, *3*, 956−970.

(4) Holder, S. J.; Sommerdijk, N. A. J. M. New micellar morphologies from amphiphilic block copolymers: disks, toroids and bicontinuous micelles. *Polym. Chem.* **2011**, *2*, 1018.

(5) Edmonds, W. F.; Li, Z.; Hillmyer, M. A.; Lodge, T. P. Disk Micelles from Nonionic Coil-Coil Diblock Copolymers. *Macromolecules* **2006**, *39*, 4526−4530.

(6) Dupont, J.; Liu, G. ABC triblock copolymer hamburger-like micelles, segmented cylin- ders, and Janus particles. *Soft Matter* **2010**, *6*, 3654.

(7) Cornwell, P. A. A review of shampoo surfactant technology: consumer benefits, raw materials and recent developments. *Int. J. Cosmet. Sci.* **2018**, *40*, 16−30.

(8) Samuel, M. M.; Card, R. J.; Nelson, E. B.; Brown, J. E.; Vinod, P. S.; Temple, H. L.; Qu, Q.; Fu, D. K. Polymer-Free Fluid for Fracturing Applications. *SPE Drill. Completion* **1999**, *14*, 240−246.

(9) Wu, X.; Song, Z.; Zhen, J.; Wang, H.; Yao, L.; Zhao, M.; Dai, C. A smart recyclable VES fluid for high temperature and high pressure fracturing. *J. Pet. Sci. Eng.* **2020**, *190*, 107097.

(10) Rodrigues, R. K.; Silva, L. A. S.; Vargas, G. G.; Loureiro, B. V. Drag Reduction by Wormlike Micelles of a Biodegradable and NonBiodegradable Surfactants. *J. Surfactants Deterg.* **2020**, *23*, 21−40.

(11) Yang, J. Viscoelastic wormlike micelles and their applications. *Curr. Opin. Colloid Interface Sci.* **2002**, *7*, 276−281.

(12) Shi, H.; Wang, Y.; Fang, B.; Talmon, Y.; Ge, W.; Raghavan, S. R.; Zakin, J. L. Light- Responsive Threadlike Micelles as Drag Reducing Fluids with Enhanced Heat-Transfer Capabilities. *Langmuir* **2011**, *27*, 5806−5813.

(13) Zhang, Y.; Chu, Z.; Dreiss, C. A.; Wang, Y.; Fei, C.; Feng, Y. Smart wormlike micelles switched by CO2 and air. *Soft Matter* **2013**, *9*, 6217.

(14) Feng, Y.; Chu, Z.; Dreiss, C. A. *Smart Wormlike Micelles Design, Characteristics and Applications*; Springer, 2015; pp. 1−91.

(15) Moore, J. E.; McCoy, T. M.; de Campo, L.; Sokolova, A. V.; Garvey, C. J.; Pearson, G.; Wilkinson, B. L.; Tabor, R. F. Wormlike micelle formation of novel alkyl-tri(ethylene glycol)-glucoside carbohydrate surfactants: Structurefunction relationships and rheology. *J. Colloid Interface Sci.* **2018**, *529*, 464−475.

(16) Kelleppan, V. T.; Moore, J. E.; McCoy, T. M.; Sokolova, A. V.; de Campo, L.; Wilkinson, B. L.; Tabor, R. F. Self-Assembly of Long-Chain Betaine Surfactants: Effect of Tailgroup Structure on Wormlike Micelle Formation. *Langmuir* **2018**, *34*, 970−977.

(17) McCoy, T. M.; King, J. P.; Moore, J. E.; Kelleppan, V. T.; Sokolova, A. V.; de Campo, L.; Manohar, M.; Darwish, T. A.; Tabor, R. F. The effects of small molecule organic addi- tives on the self-assembly and rheology of betaine wormlike micellar fluids. *J. Colloid Interface Sci.* **2019**, *534*, 518−532.

(18) Jiang, H.; Vogtt, K.; Thomas, J. B.; Beaucage, G.; Mulderig, A. Enthalpy and Entropy of Scission in Wormlike Micelles. *Langmuir* **2018**, *34*, 13956−13964.

(19) Abdel-Rahem, R. A.; Reger, M.; Hloucha, M.; Hoffmann, H. Rheology of Aqueous Solu- tions Containing SLES, CAPB, and Microemulsion: Influence of Cosurfactant and Salt. *J. Dispersion Sci. Technol.* **2014**, *35*, 64−75.

(20) Vogtt, K.; Beaucage, G.; Weaver, M.; Jiang, H. Thermodynamic stability of worm-like micelle solutions. *Soft Matter* **2017**, *13*, 6068−6078.

(21) Sokolova, A.; Christoforidis, J.; Eltobaji, A.; Barnes, J.; Darmann, F.; Whitten, A. E.; de Campo, L. BILBY: Time-of-Flight Small Angle Scattering Instrument. *Neutron News* **2016**, *27*, 9−13.

(22) Sokolova, A.; Whitten, A. E.; de Campo, L.; Christoforidis, J.; Eltobaji, A.; Barnes, J.; Darmann, F.; Berry, A. Performance and characteristics of the BILBY time-of-flight small-angle neutron scattering instrument. *J. Appl. Crystallogr.* **2019**, *52*, 1−12.

(23) Rehm, C.; de Campo, L.; Brûlé, A.; Darmann, F.; Bartsch, F.; Berry, A. Design and performance of the variable-wavelength

BonseHart ultra-small-angle neutron scattering diffractometer KOOKABURRA at ANSTO. *J. Appl. Crystallogr.* **2018**, *51*, 1−8.
(24) Kline, S. R. Reduction and analysis of SANS and USANS data using IGOR Pro. *J. Appl. Crystallogr.* **2006**, *39*, 895−900.
(25) Chen, W. R.; Butler, P. D.; Magid, L. J. Incorporating intermicellar interactions in the fitting of SANS data from cationic wormlike micelles. *Langmuir* **2006**, *22*, 6539−6548.
(26) Moore, J. E.; McCoy, T. M.; Sokolova, A. V.; de Campo, L.; Pearson, G. R.; Wilkinson, B. L.; Tabor, R. F. Worm-like micelles and vesicles formed by alkyl-oligo(ethylene glycol)-glycoside carbohydrate surfactants: The effect of precisely tuned amphiphilicity on aggregate packing. *J. Colloid Interface Sci.* **2019**, *547*, 275−290.
(27) Helgeson, M. E.; Vasquez, P. A.; Kaler, E. W.; Wagner, N. J. Rheology and spatially resolved structure of cetyltrimethylammonium bromide wormlike micelles through the shear banding transition. *J. Rheol.* **2009**, *53*, 727−756.
(28) Das, N. C.; Cao, H.; Kaiser, H.; Warren, G. T.; Gladden, J. R.; Sokol, P. E. Shape and Size of Highly Concentrated Micelles in CTAB/NaSal Solutions by Small Angle Neutron Scattering (SANS). *Langmuir* **2012**, *28*, 11962−11968.
(29) Calabrese, M. A.; Rogers, S. A.; Porcar, L.; Wagner, N. J. Understanding steady and dynamic shear banding in a model wormlike micellar solution. *J. Rheol.* **2016**, *60*, 1001−1017.
(30) Lequeux, F. Structure and rheology of wormlike micelles. *Curr. Opin. Colloid Interface Sci.* **1996**, *1*, 341−344.
(31) Bonneté, F.; Vivarès, D.; Robert, C.; Colloc'h, N. Interactions in solution and crys- tallization of Aspergillus flavus urate oxidase. *J. Cryst. Growth* **2001**, *232*, 330−339.
(32) Couillet, I.; Hughes, T.; Maitland, G.; Candau, F.; Candau, S. J. Growth and Scission Energy of Wormlike Micelles Formed by A Cationic Surfactant with Long Unsaturated Tails. *Langmuir* **2004**, *20*, 9541−9550.
(33) Teixeira, J. Small-angle scattering by fractal systems. *J. Appl. Crystallogr.* **1988**, *21*, 781−785.
(34) Wei, X.-L.; Han, C.-H.; Geng, P.-P.; Chen, X.-X.; Guo, Y.; Liu, J.; Sun, D.-Z.; Zhang, J.-H.; Yu, M.-J. Thermo-responsive properties driven by hydrogen bonding in aqueous cationic gemini surfactant systems. *Soft Matter* **2016**, *12*, 1558−1566.
(35) Cardiel, J. J.; Dohnalkova, A. C.; Dubash, N.; Zhao, Y.; Cheung, P.; Shen, A. Q. Microstructure and rheology of a flow-induced structured phase in wormlike micellar solutions. *Proc. Natl. Acad. Sci. U. S. A.* **2013**, *110*, E1653−E1660.

https://dx.doi.org/10.1021/acs.langmuir.0c02530
Langmuir XXXX, XXX, XXX−XXX